epl draft

Coulomb Drag and High Resistivity Behavior in Double Layer Graphene

N. M. R. Peres[1], J. M. B. Lopes dos Santos[2] and A. H. Castro Neto[3,4]

[1] *Department of Physics and Center of Physics, University of Minho, P-4710-057, Braga, Portugal, EU*
[2] *CFP and Departamento de Física, Faculdade de Ciências Universidade do Porto, P-4169-007 Porto, Portugal, EU*
[3] *Graphene Research Centre and Physics Department, National University of Singapore, 2 Science Drive 3, Singapore 117541*
[4] *Department of Physics, Boston University, 590 Commonwealth Avenue, Boston, MA 02215, USA*

PACS 81.05.ue – Graphene
PACS 72.80.Vp – Electronic transport in graphene

Abstract –We show that Coulomb drag in ultra-clean graphene double layers can be used for controlling the on/off ratio for current flow by tunning the external gate voltage. Hence, although graphene remains semi-metallic, the double layer graphene system can be tuned from conductive to a highly resistive state. We show that our results explain previous data of Coulomb drag in double layer graphene samples in disordered SiO_2 substrates.

Introduction. – Coulomb drag, as represented in Fig. 1, is the phenomenon where a voltage V_2 applied to a two-dimensional (2D) conducting layer (called the active layer) generates both a current I_2 on that plane and a voltage V_1 in another layer, parallel to the first, and located at a distance d [1]. This effect occurs because electrons in the active layer, under the presence of an electric field E_2, "drag" the electrons in the other layer through their mutual Coulomb interaction. The current densities in each layer, j_1 and j_2, are related to electric fields in each layer through the conductivity tensor, according to the general relation:

$$\begin{bmatrix} j_1 \\ j_2 \end{bmatrix} = \begin{pmatrix} \sigma_{11} & \sigma_D \\ \sigma_D & \sigma_{22} \end{pmatrix} \begin{bmatrix} E_1 \\ E_2 \end{bmatrix} \equiv \bar{\sigma} \begin{bmatrix} E_1 \\ E_2 \end{bmatrix} , \quad (1)$$

where σ_{ii} is the conductivity of each isolated layer ($d \to \infty$) and σ_D is the so-called trans-conductivity. Notice that in a drag experiment no current flows in the non-active sheet, that is, $j_1 = 0$, and hence we can express the electric fields E_1 and E_2 in terms of the current j_2 in the active plane alone. This allow us to define the quantities of experimental interest, namely the drag resistivity ρ_D, given by

$$\rho_D = \frac{WV_1}{I_2 L} = \frac{E_1}{j_2} = -\frac{\sigma_D}{\det\bar{\sigma}} , \quad (2)$$

and the longitudinal resistivity ρ_L, reading

$$\rho_L = \frac{E_2}{j_2} = \frac{\sigma_{11}}{\det\bar{\sigma}} , \quad (3)$$

where $\det\bar{\sigma} = \sigma_{11}\sigma_{22} - \sigma_D^2$ is the determinant of conductivity tensor $\bar{\sigma}$ (W is the width and L is the length of the device).

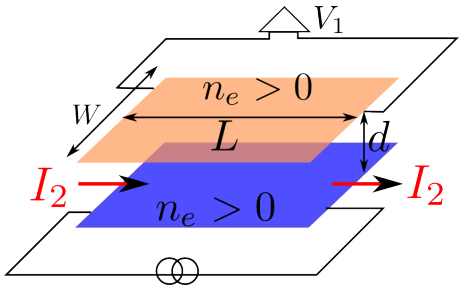

Fig. 1: Generic representation of a Coulomb drag experiment.

Using the above equations we can eliminate the trans-conductivity in terms of ρ_D and rewrite the relationship between the drag and the longitudinal resistivities as:

$$\rho_L = \frac{2\rho_D^2/\rho_1}{\sqrt{1 + 4\rho_D^2/(\rho_1\rho_2)} - 1} , \quad (4)$$

where $\rho_i = 1/\sigma_{ii}$. Eq. (4) has two extreme limits:

$$\rho_L \approx \begin{cases} \rho_2 + \rho_D^2/\rho_1 , & \rho_D \ll \sqrt{\rho_1\rho_2}/2 , \\ \sqrt{\rho_2/\rho_1}\rho_D , & \rho_D \gg \sqrt{\rho_1\rho_2}/2 . \end{cases} \quad (5)$$

Hence, in the limit where the drag resistivity is small compared with the resistivity of the two layers ($\rho_D \ll \sqrt{\rho_1\rho_2}/2$) the longitudinal resistivity is dominated by the resistivity of the active layer. This is the usual case of the 2D electron gases (2DEG), found in semiconducting heterostructures [2–4], where the drag resistance is a small effect.

In what follows, we will argue that for the case of an ultra-clean graphene double layer the opposite regime can be reached, namely, one can have $\rho_D \gg \sqrt{\rho_1\rho_2}/2$ with $\rho_1 \ll \rho_2$ so that the longitudinal resistivity, ρ_L, is proportional to the drag resistivity, but enhanced by a factor proportional to $\sqrt{\rho_2/\rho_1} \gg 1$, so that $\rho_L \gg \rho_D \gg \sqrt{\rho_1\rho_2}/2$. This regime can be reached in ultra-clean graphene by tuning the bottom and top gates in the device (see Fig. 1) such that the Fermi energy of the non-active layer, $\epsilon_{F1} = v_F k_{F1}$ (where $v_F \approx 10^6$ m/s is the Fermi velocity), is large, but the Fermi energy of the active layer, $\epsilon_{F2} = v_F k_{F2}$, is small and close to the neutrality point (that is, one requires that $k_{F1} \gg k_{F2}$). This is only possible in graphene because the resistivity in each individual graphene layer is a monotonically decreasing function of the density, $|n_e|$, in each plane ($k_{Fi} = \sqrt{\pi|n_e|}$) [5]. In ultra-clean graphene, the resistivity is a very sharp function of the density and therefore the longitudinal resistivity can be enhanced by orders of magnitude by the drag effect. In fact, we show that the drag resistance diverges at low densities as $\rho_D \sim n_e^{-0.8}$ ($n_e \to 0$) and therefore the longitudinal resistance can become arbitrarily large. We stress that the behavior for ρ_D, as computed using our model, is better described by the relation $\rho_D \sim n_e^{-\alpha(n_e)}$, where the exponent $\alpha(n_e)$ is a function of n_e and shows a crossover from $\alpha \simeq 2$ to $\alpha \simeq 1$ as n_e decreases.

The mechanism described here can produce a huge enhancement of the on-and-off ratio for current flow in graphene, without the need for the opening of a gap in the spectrum, solving the famous bottleneck for the use of graphene devices in high end electronic applications.

While we wait for the drag data in ultra-clean samples [6], we check our model against the existing data for drag resistivity measurements in graphene on SiO_2 [7]. As it is well known, SiO_2 is a dirty substrate, and at low densities electron-hole puddles are formed [8,9], greatly limiting the mobility in these devices. We show that our model applies to this conventional case describing the data extremely well.

We notice that the theoretical literature on Coulomb drag in graphene is scarce [10, 11], and it was shown [7] that the theoretical approaches used so far [10,11] are unable to describe the experimental data. Under a number of simplifying assumptions, it was shown [11] that electrons in graphene, when described by the massless Dirac equation, should have zero drag-resistivity. According to that analysis [11], trigonal warping corrections would be necessary to explain a finite drag resistivity in graphene. We show here that such is not the case when the momentum dependence of the scattering time is taken into account and dynamic effects in Coulomb screening are correctly included.

Theory of Coulomb drag and experimental results. – The drag resistivity can be obtained from the solution of Boltzmann's kinetic equation [12–16]. In this approach it is assumed that the main scattering mechanism within a graphene layer is electron-impurity scattering [17, 18] and that the electronic density is outside the range where one finds electron-hole puddles [8,9]. In dirty substrates such as SiO_2 this can happen at densities of 10^{12} cm^{-2}, however, in cleaner substrates such as Boron-Nitride [19] this only happens at extremely low densities of the order of 10^{10} cm^{-2} [20]. Without loss of generality we also assume that the graphene layers are electron doped and, as explained above, the Fermi energy in the two graphene layers is such that $\epsilon_{F2} \leq \epsilon_{F1}$. We also make use of the full dynamical screening between the layers, which takes into account intra- as well as inter-layer interactions. However, in calculating the resistivity we only take into account intra-band interactions between electrons belonging to each of the sheets (the validity of this assumption is achieved by keeping the electronic density large enough [11]). Finally, one key point of our approach is taking into account the full momentum dependence of the electronic scattering time $\tau_{\boldsymbol{k}}$, originated from electron-impurity scattering. It is well known that $\tau_{\boldsymbol{k}}$ is roughly proportional to the square root of the electronic density, that is, we have $\tau_{\boldsymbol{k}} = \tau_0 k$, where τ_0 is a constant computed elsewhere [17], and which drops out at the end of the calculation. This assumption is in agreement with the experimental data [5] and is essential for the accurate description of Coulomb drag in graphene.

Within these assumptions, Boltzmann's kinetic equation suffices for the description of the drag resistivity. The final result for the latter quantity (and the central result of this paper; see derivation ahead) is

$$\begin{aligned} \rho_D &= -\frac{1}{g_0}\frac{\sqrt{\epsilon_{F1}\epsilon_{F2}}}{2^5\pi k_B T}\alpha_c^2 \mathcal{F}(k_{F2}, k_{F1}, T, d_c, \alpha_g) \\ &\equiv -\rho_0 \mathcal{F}(k_{F2}, k_{F1}, T, d_c, \alpha_g)\,. \end{aligned} \tag{6}$$

The reader is referred to the derivation of Eq. (24) for the definition of the several quantities in Eq. (6). Using Eq. (6) we are able to describe quantitatively the drag resistivity measured in graphene at different temperatures [7]. Our results are summarized in Fig. 2. In that figure the symbols are the experimental data and the dashed lines are the calculated values of ρ_D. The drag resistivity is represented as function of the gate voltage. The calculated curves have been horizontally shifted by $V_D = -2$ V, since the graphene in the device had its neutrality point at $V_g = V_D$, whereas the calculated curves assume neutral graphene when $V_g = 0$. The agreement is quantitative up to $V_g = 4$; below we discuss the origin of the deviations for $V_g < 4$ V, which are associated with the electron-puddle formation in the device. To understand the experimental

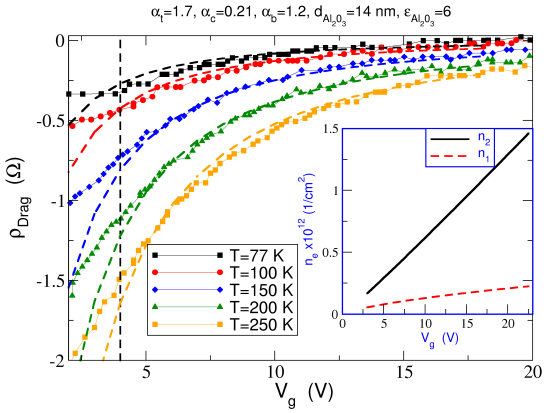

Fig. 2: Calculation of the drag resistivity as function of the gate-voltage and comparison with the experimental measurements [7], using $\alpha_c = 0.21$, $d_b = 280$ nm, $\epsilon_b = 3.8$, $d_t = 14$ nm, and $\epsilon_t = 6$. Note that except for α_c, the parameters d_b, d_t, ϵ_b, and ϵ_t are a characteristic of the apparatus used in the experiment, and therefore fixed numbers. The symbols are the experimental data and the dashed lines are the calculated values of ρ_D. The inset represents the electronic density, n_1 and n_2, in the two sheets, as obtained from the solution of Eqs. (7) and (8). We note that n_1 and n_2 are not independent of each other.

conditions associated with the measurements reproduced in Fig. 2 the reader is referred to Ref. [7].

The device has two different dielectrics: SiO_2 (relative permittivity $\epsilon_b = 3.8$), with thickness $d_b = 280$ nm, and Al_2O_3 (relative permittivity $\epsilon_t = 6$ [21]), with thickness $d_t = 14$ nm (we note that other authors report a value of $\epsilon_{Al_2O_3} = 9.1$ [22]). The latter oxide is sandwiched between the two graphene layers. As detailed in Ref. [7], the densities in the two layers are not independent of each other. The electronic densities n_2 and n_1 follow from [7]:

$$eV_g = d_b \frac{e^2}{\epsilon_0 \epsilon_b}(n_2 + n_1) + v_F \hbar \sqrt{\pi n_2}\,, \qquad (7)$$

$$d_t \frac{e^2}{\epsilon_0 \epsilon_t} n_1 = v_F \hbar (\sqrt{\pi n_2} - \sqrt{\pi n_1})\,. \qquad (8)$$

The numerical solution of the last two equations gives the electronic density in the two graphene sheets for any value of V_g (see inset in Fig. 2).

In our theory, the only free parameter is the intrinsic dielectric of constant graphene or, equivalently, the interaction parameter:

$$\alpha_g = \frac{e^2}{4\pi\epsilon_0 v_F \hbar} \approx 2.2\,. \qquad (9)$$

We note that there is some controversy on the value of α_g [23]. When graphene is immersed in a dielectric of relative permittivity ϵ_r, the interaction parameter becomes $\alpha_r = \alpha_g/\epsilon_r$. In the experimental setup [7] there are three different interaction parameters: two associated with electron-electron interactions within the two graphene planes (α_t and α_b) and one associated with the inter-plane interaction (α_c). The constants α_t and α_b play their role in the calculation of the dielectric function of the coupled layers. Explicitly, we have:

$$\alpha_t = 2\alpha_g/(1 + \epsilon_{Al_2O_3})\,, \qquad (10)$$

$$\alpha_c = \alpha_g/\epsilon_{Al_2O_3}\,, \qquad (11)$$

$$\alpha_b = 2\alpha_g/(\epsilon_{Al_2O_3} + \epsilon_{SiO_2})\,. \qquad (12)$$

Taking α_c as reference, we get $\alpha_t \simeq 1.7\alpha_c$ and $\alpha_b \simeq 1.2\alpha_c$; these two numbers are fixed in our model. Therefore, the only free parameter is α_g, or in alternative α_c. We have chosen α_c as our fitting parameter and the best fit was obtained for $\alpha_c = 0.21$. This latter value implies:

$$\alpha_g \simeq 1.3\,, \qquad (13)$$

a number close to the one given by Eq. (9).

The vertical dashed line in Fig. 2 sets the limit of validity of our theoretical model in what concerns its application to graphene on dirty substrates. Indeed, at that point the experimental curves change their curvature from negative to positive, indicating a change of regime. Below $V_g = 4$ V, the theoretical results start to deviate from the measured data. This happens because the electronic density in the bottom layer approaches the regime where electron-hole puddles control the electronic transport in graphene [7]. In fact, looking at the green curve of Fig. 3.a in Ref. [7], we see that during the transition from the regime of electron-electron drag to that of electron-hole drag the behavior of ρ_D is reminiscent of that reported for Hall-measurements in graphene close to the neutrality point [5]. In both cases, the elementary theory, which ignores the effect of electron-hole puddles, predicts diverging drag resistivity and Hall coefficient. We note that our computed curves diverge as the electronic density is reduced; the divergence is enhanced at high temperatures. In the absence of electron-hole puddles ρ_D can become large, giving rise to the switching effect we have described in the introduction.

Derivation of the drag resistivity formula. – The calculation of the current density j_2 (the driven current) and the electric field E_1 (the drag field) requires the solution of Boltzmann's equation, under the assumption that the current density in sheet **1** is zero, $j_1 = 0$. The driven current j_2 reads

$$j_2 = E_2 g_0 \pi v_F \tau_0 n_2\,. \qquad (14)$$

Following a standard procedure [14–16], the drag field E_1 is given by:

$$E_1 = \frac{1}{g_0}\frac{e_1 g_s g_v}{\pi n_1}\int \frac{d\boldsymbol{k}_1}{4\pi^2} k_1 \cos\theta_{\boldsymbol{k}_1} \left.\frac{\partial f_{\boldsymbol{k}_1,c}}{\partial t}\right]_{\rm ee}\,, \qquad (15)$$

where $\partial f_{\boldsymbol{k}_1,c}/\partial t]_{\rm ee}$ is the collision integral due to inter-plane Coulomb interactions, e_1 is the charge of the carriers

in plane **1**, $g_0 = 2e^2/h$, n_1 is the electronic density in layer **1**, and g_s and g_v are the spin and valley degeneracy, respectively. We stress that unlike previous works [10] we take fully into account the momentum dependence of the relaxation time. It was noted before that ignoring this momentum dependence leads to incorrect results [16] (for the 2DEG, however, the relaxation time can be taken momentum independent).

The calculation of the collision integral requires the use of the Coulomb interaction between electrons in different layers. The latter is given by

$$H_{12} = \frac{1}{4A}\sum_{\boldsymbol{k}_1,\boldsymbol{k}_2,\boldsymbol{q}}\sum_{\alpha,\alpha',\beta,\beta'} U_{d_c}(\boldsymbol{q}) f_{\alpha\alpha'}(\boldsymbol{k}_1,\boldsymbol{q}) f_{\beta\beta'}(\boldsymbol{k}_2,\boldsymbol{q}) \times a^\dagger_{\boldsymbol{k}_1\alpha} a_{\boldsymbol{k}_1+\boldsymbol{q}\alpha'} b^\dagger_{\boldsymbol{k}_2\beta} b_{\boldsymbol{k}_2-\boldsymbol{q}\beta'} , \quad (16)$$

where the creation operators $a^\dagger_{\boldsymbol{k}_1\alpha}$ and $b^\dagger_{\boldsymbol{k}_2\alpha}$ refer to electrons in layers **1** and **2**, respectively, A is the area of the system, and

$$U_{d_c}(\boldsymbol{q}) = \frac{e_1 e_2}{2\epsilon_c\epsilon_0 q} e^{-qd_c} \equiv V_c(q) e^{-qd_c} , \quad (17)$$

where d_c is the inter-layer distance. The transferred momentum between the layers is $\boldsymbol{q} = \boldsymbol{k}_1 - \boldsymbol{k}_2$, $\alpha, \alpha', \beta, \beta' = v, c$ refer to the valence (v or -1) and conduction (c or +1) band electrons, the momentum of electrons in plane **1** is denoted by $\boldsymbol{k}_1$ and for electrons in plane **2** by $\boldsymbol{k}_2$; the momentum sums $\boldsymbol{k}_1$ and $\boldsymbol{k}_2$ contain spin summations as well. The chiral nature of the electron wave function is encoded in the form factors:

$$f_{\alpha\alpha'}(\boldsymbol{k}_1,\boldsymbol{q}) = 1 + \alpha\alpha' e^{i(\theta_{\boldsymbol{k}_1} - \theta_{\boldsymbol{k}_1+\boldsymbol{q}})} , \quad (18)$$

$$f_{\beta\beta'}(\boldsymbol{k}_2,\boldsymbol{q}) = 1 + \beta\beta' e^{i(\theta_{\boldsymbol{k}_2} - \theta_{\boldsymbol{k}_2-\boldsymbol{q}})} , \quad (19)$$

where $\theta = \arctan(k_y/k_x)$.

Following a standard approach [14–16, 24], we have

$$\int \frac{d\boldsymbol{k}_1}{4\pi^2} k_1 \cos\theta_{\boldsymbol{k}_1} \frac{\partial f_{\boldsymbol{k}_1,c}}{\partial t}\Big]_{\rm ee} = -E_2 \frac{\pi e v_F \tau_0}{2\hbar k_B T} \times \int \frac{d\boldsymbol{q}}{4\pi^2} \int \hbar d\omega \frac{|U(\boldsymbol{q},\omega)|^2}{\sinh^2(\hbar\omega/2k_BT)} P_{1c}(\boldsymbol{q},\omega) P_{2c}(\boldsymbol{q},\omega) , \quad (20)$$

where $U(\boldsymbol{q},\omega) = U_{d_c}(q)/\epsilon(\boldsymbol{q},\omega)$ is the dynamic Coulomb interaction, evaluated using the random phase approximation for the dynamic dielectric function $\epsilon(\boldsymbol{q},\omega)$. We note that τ_0 is not the relaxation time (see above), and it cancels out when the ratio E_1/j_2 is computed. We also have

$$P_{jc}(q,\omega) = \int \frac{d\boldsymbol{k}_1}{4\pi^2} G^{(j)}_{\boldsymbol{k}_j,\boldsymbol{q}} \delta f_{\boldsymbol{k}_j,\boldsymbol{q}} \delta(\hbar\omega + \hbar\omega_{\boldsymbol{k}_j,\boldsymbol{q}}) , \quad (21)$$

where $\delta f_{\boldsymbol{k}_j,\boldsymbol{q}} = f_{\boldsymbol{k}_j+\boldsymbol{q}/2} - f_{\boldsymbol{k}_j-\boldsymbol{q}/2}$, $\hbar\omega_{\boldsymbol{k}_j,\boldsymbol{q}} = \epsilon_{\boldsymbol{k}_j-\boldsymbol{q}/2} - \epsilon_{\boldsymbol{k}_j+\boldsymbol{q}/2}$ ($j = 1, 2$), and the function $G^{(j)}_{\boldsymbol{k}_1,\boldsymbol{q}}$, with $j = 1, 2$, is defined as

$$G^{(j)}_{\boldsymbol{k}_j,\boldsymbol{q}} = \frac{1}{2+2\delta_{1,j}} \left[|\boldsymbol{k}_j - \boldsymbol{q}/2| \cos\theta_{\boldsymbol{k}_j-\boldsymbol{q}/2} - |\boldsymbol{k}_j + \boldsymbol{q}/2| \cos\theta_{\boldsymbol{k}_j+\boldsymbol{q}/2} \right] |f_{cc}(\boldsymbol{k}_j,\boldsymbol{q})|^2 . \quad (22)$$

The difference between our calculation and that of Tse *et al.* [10] is precisely in the form of the $G^{(j)}_{\boldsymbol{k}_j,\boldsymbol{q}}$. The dynamic dielectric function $\epsilon(\boldsymbol{q},\omega)$ for the two-layer system is given by [16, 25]:

$$\epsilon(\boldsymbol{q},\omega) = \epsilon_2(\boldsymbol{q},\omega)\epsilon_1(\boldsymbol{q},\omega) - U^2_{d_c}(q)\mathcal{P}_1(\boldsymbol{q},\omega)\mathcal{P}_2(\boldsymbol{q},\omega) , \quad (23)$$

where $\epsilon_j(\boldsymbol{q},\omega) = 1 - V_j(\boldsymbol{q})\mathcal{P}_j(\boldsymbol{q},\omega)$ and $\mathcal{P}_j(\boldsymbol{q},\omega)$ are the dielectric and polarization functions of each of the individual layers [26]. Notice that α_b and α_t enter in $\epsilon_b(\boldsymbol{q},\omega)$ and $\epsilon_t(\boldsymbol{q},\omega)$, respectively. Once the functions $P_{jc}(q,\omega)$ are computed, a relatively simple expression follows for the drag resistivity:

$$\rho_D = -\frac{1}{g_0} \frac{\sqrt{\epsilon_{F1}\epsilon_{F2}}}{2^5\pi k_B T} \alpha_c^2 \mathcal{F}(k_{F2}, k_{F1}, T, d_c, \alpha_g) , \quad (24)$$

which leads to Eq. (6) and α_c is the interaction parameter of graphene considering the dielectric in between the two graphene layers made out of Al_2O_3. The dimensionless function $\mathcal{F}(k_{F2}, k_{F1}, T, d_c, \alpha_g)$ is defined as:

$$\mathcal{F}(k_{F2}, k_{F1}, T, d_c, \alpha_g) = \sum_{m=1}^{3} \int_0^{x_{\rm m}} dx \int_0^{y_{\rm m}} dy F(x,y) , \quad (25)$$

where

$$F(x,y) = \frac{x^9(x^2-y^2)}{|\epsilon(x,y)|^2} \frac{\Phi_1(x,y)\Phi_2(x,y)}{\sinh^2 \frac{v_F\hbar\sqrt{k_{F1}k_{F2}}y}{2k_BT}} e^{-2d_c x\sqrt{k_{F1}k_{F2}}} , \quad (26)$$

and x and y are dimensionless variables defined as $q = \sqrt{k_{F1}k_{F2}}x$ and $\omega = v_F\sqrt{k_{F1}k_{F2}}y$, respectively. The three integration regions are: $0 < x_1 < b$, $0 < y_1 < \min(x, -x + b)$; $b/2 < x_2 < (a+b)/2$, $\max(-x+b, x-b) < y_2 < \min(x, -x+a)$; $a/2 < x_3 < \infty$, $\max(-x+a, x-b) < y_3 < q$ where $a = 2\sqrt{k_{F1}/k_{F2}}$ and $b = 2\sqrt{k_{F2}/k_{F1}}$. The function $\epsilon(x,y)$ is defined as:

$$\epsilon(x,y) = (x\sqrt{x^2-y^2} + P_{12})(x\sqrt{x^2-y^2} + P_{21}) - P_{12}P_{21}e^{-2d_c\sqrt{k_{F1}k_{F2}}x} , \quad (27)$$

where

$$P_{sj} = 4\alpha_s \sqrt{\frac{k_{Fs}}{k_{Fj}}} \sqrt{x^2-y^2} - i\frac{\alpha_s}{2} x^2 \Phi_s(x,y) , \quad (28)$$

and α_s equals α_b or α_t, depending on the graphene layer. Below we outline the calculation of the functions $\Phi_s(x,y)$.

In Fig. 3 we plot the quantity $\rho_0 F(x,y)$ for particular values of k_{Fi} (as determined by the gate voltage), the effective interaction parameter α_c, the distance between the two layers, and the temperature. In that figure the three panels, from top to bottom, represent the contribution of the three integration domains defined by x_m and y_m. At low temperatures and high back-gate voltage, only the contribution of region $m = 1$ is significant; on the other hand, at high temperature and low densities all the three regions ($m = 1, 2, 3$) give a significant contribution to ρ_D, as shown with the example in Fig. 3.

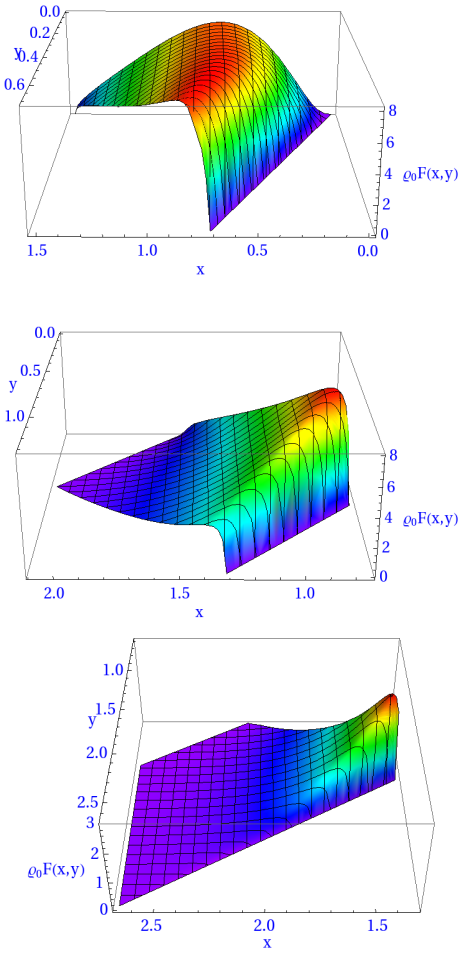

Fig. 3: Plot of the integration kernel $\rho_0 F(x,y)$ in Eq. (25) for the parameters $V_g = 3$ V, $d = 14$ nm, $\alpha_g = 0.21$, and $T = 300$ K. The three figures correspond to three different regions of the (q, Ω) plane. From top to bottom the regions are ordered as m =1, m =2, and m =3 (see text).

Particular limits of ρ_D. – Let us now consider the case where α_b, α_c, and α_t are all equal, as is the electronic density in the two sheets. Taking the limit of very low densities, we see that ρ_D can reach values of the order of 10^3 Ω, as in the case represented in Fig. 4. It is the possibility of having large values of ρ_D that suggests the mechanism for turning *on*-and-*off* the electric current in a double-layer graphene-based transistor. We also note that in the density range $n_e \sim 3\times10^{12}$ cm^{-2} to $n_e \sim 0.5\times10^{12}$ cm^{-2}, ρ_D is better described by $\rho_D \propto n_e^{-\alpha(n_e)}$, where the exponent $\alpha(n_e)$ shows a crossover from $\alpha(n_e) \simeq 2$ to $\alpha(n_e) \simeq 1$ as the electronic density is reduced.

Finally, when $\epsilon_F \gg k_B T$ and $d_c k_F \gg 1$, the asymptotic regime for ρ_D reads

$$\rho_D \propto -\frac{1}{g_0}\frac{(k_B T)^2}{v_F^2 \hbar^2 n_e^4 d_c^6}\,. \tag{29}$$

The asymptotic formula (29) has a different dependence on

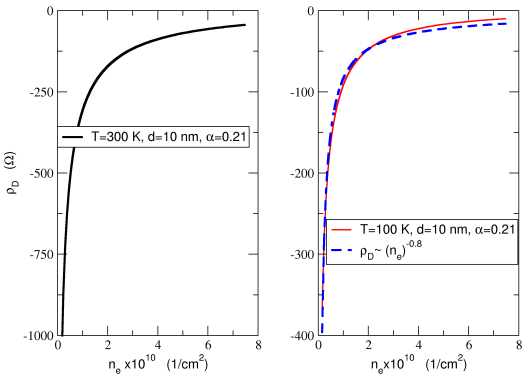

Fig. 4: Dependence of the drag resistivity on the density for two different temperatures, $T = 300$ K and $T = 100$ K. The other parameters are $\alpha_b = \alpha_c = \alpha_t = 0.21$, $d_b = d_t = 280$ nm, and $d_c = 10$ nm. The dashed curve is a fit to the expression $\rho_D \propto n_e^{-0.8}$.

d and n_e from that found in Ref. [10], due to the inclusion of the momentum dependence in the scattering time; in Ref. [10] the integration over q has a kernel of the form $q^3/\sinh^2(qd_c)$, whereas our kernel, in the same limit, has the form $q^5/\sinh^2(qd_c)$. Thus we obtain $\rho_D \propto d^6$ and Tse *et al.* have obtained $\rho_D \propto d^4$. The difference by a factor of two in the power of the momentum q comes from: (i) $\tau_{\boldsymbol{q}} \propto q$; (ii) $\tau_{\boldsymbol{q}}$ appears twice in the right-hand side of Eq. (15). It is worth stressing that Eq. (29) does not apply to the conditions of the experiment we have described in Fig. 2, and the experimental conditions where it would apply can hardly be reached. Also, the values of ρ_D of an experiment done in the regime of validity of Eq. (29) would be difficult to measure.

Technical details: Calculation of the functions $\Phi_j(x,y)$ at zero temperature. – The functions $\Phi_j(x,y)$ – $j = 1, 2$ – depend on the integration limits x_i and y_i – $i = 1, 2, 3$; we also define $\Omega = \omega/v_F$. We write $\Phi_j(q,\Omega,k_{Fj}) = \Phi_j^+(q,\Omega,k_{Fj}) + \Phi_j^-(q,\Omega,k_{Fj})$, where

$$\Phi_j^\pm(q,\Omega,k_{Fj}) = \int_{-\infty}^{\infty} d\phi \sinh^2\phi f_j[(q\cosh^2\phi \pm \Omega)/2]\,. \tag{30}$$

At zero temperature we have:

$$f_j[(q\cosh^2\phi \pm \Omega)/2] = \theta[2k_{Fj} - (q\cosh^2\phi \pm \Omega)]\,. \tag{31}$$

In terms of the functions $\Phi_j^+(q,\Omega,k_{Fj})$ and $\Phi_j^-(q,\Omega,k_{Fj})$, the function $\Phi_j(q,\Omega,k_{Fj})$ reads:

1. **region 1:** $0 < q < k_{Fj}$ and $0 < \Omega < q$, in which case we have $\Phi_j = \Phi_j^+ - \Phi_j^-$ (we have omitted the arguments of the functions $\Phi_j(q,\Omega,k_{Fj})$ for the sake of simplicity);

2. **region 2:** $k_{Fj} < q < 2k_{Fj}$ and $0 < \Omega < 2k_{Fj} - q$, in which case we have $\Phi_j = \Phi_j^+ - \Phi_j^-$;
3. **region 3:** $k_{Fj} < q < 2k_{Fj}$ and $2k_{Fj} - q < \Omega < q$, in which case we have $\Phi_j = -\Phi_j^-$;
4. **region 4:** $q > 2k_{Fj}$ and $q - 2k_{Fj} < \Omega < q$, in which case we have $\Phi_j = -\Phi_j^-$.

In the regions where $\Phi_j^\pm$ is finite we have

$$\Phi_j^+(q,\Omega,k_{Fj}) = -\phi_{\min} + \frac{1}{2}\sinh(2\phi_{\min}), \quad (32)$$

$$\Phi_j^-(q,\Omega,k_{Fj}) = -\phi_{\max} + \frac{1}{2}\sinh(2\phi_{\max}), \quad (33)$$

where $\phi_{\max} = \operatorname{arccosh}[(2k_{Fj}+\Omega)/q]$ and $\phi_{\min} = \operatorname{arccosh}[(2k_{Fj}-\Omega)/q]$. The four regions above have their

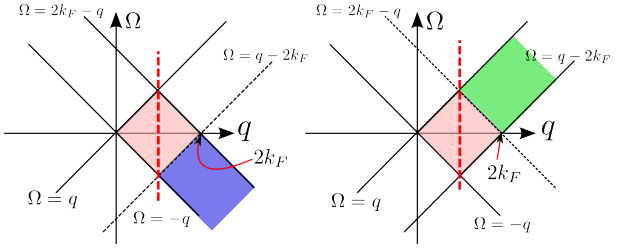

Fig. 5: Domains where the functions $\Phi_j^+(q,\Omega,k_{Fj})$ (left) and $\Phi_j^-(q,\Omega,k_{Fj})$ (right) are finite. In the triangular area, both functions are finite. In the rectangular area only one of the functions is finite.

graphical representation in Fig. 5. In the triangular area of the diagram 5, the polarization reads

$$\mathcal{P}_j(\boldsymbol{q},\Omega) = -\frac{2k_{Fj}}{\pi v_F \hbar} + \frac{i}{4\pi v_F \hbar}\frac{q^2}{\sqrt{q^2-\Omega^2}}\Phi_j(\boldsymbol{q},\Omega). \quad (34)$$

In the rectangular area of the same diagram, the polarization is obtained by adding to Eq. (34) the term

$$\frac{1}{4\pi v_F \hbar}\frac{1}{\sqrt{q^2-\Omega^2}}\Theta_j(\boldsymbol{q},\Omega), \quad (35)$$

where $\Theta_j(\boldsymbol{q},\Omega) = \Theta_a(\boldsymbol{q},\Omega) + \Theta_b(\boldsymbol{q},\Omega)$ and

$$\Theta_a(\boldsymbol{q},\Omega) = (2k_{Fj}-\Omega)\sqrt{q-2k_{Fj}+\Omega}\times \sqrt{q+2k_{Fj}-\Omega}, \quad (36)$$

$$\Theta_b(\boldsymbol{q},\Omega) = -2q^2 \arctan\sqrt{\frac{q+\Omega-2k_{Fj}}{q-\Omega+2k_{Fj}}}. \quad (37)$$

We have used these results for the polarization in the calculation of the dynamic dielectric function.

Conclusions. – We have given a quantitative theory of Coulomb drag in graphene. We have shown that for ultra-clean graphene, unlike the case of a conventional 2DEG, can be tuned to a region of diverging drag and longitudinal resistivity allowing the use of double layer structures for device applications where the on-and-off ratio for the current flow has to be large. We also show that our theory explains quantitatively the experimental data for the drag resistivity in dirty devices away from the electron-hole puddle region. As this region shrinks in cleaner devices, the validity of our theory extends.

Supplementary Information. – In Fig. 6 we plot the dependence of the drag resistivity as function of the electronic density, n_e, the interlayer distance, d_c, and the temperature, T. The density range scanned in this figure is different from that given in Fig. 4. In the three panels of Fig. 6 the black dashed lines are fits to a power law of the form $\rho_D \sim x^{\alpha_x}$, where x represents one of three parameters n_e, d_c, and T. From these fits we have found that ρ_D follows, in the regime of parameters of Fig. 6, roughly the behavior

$$\rho_D \sim \frac{(Tk_B)^2}{v_F^2\hbar^2 n_e^2 d_c^2}. \quad (38)$$

It is also clear from Fig. 6 that Eq. (38) holds only approximately. Also, comparing the dependence of ρ_D on n_e, as given in the regime of parameters of Fig. 4, with that of Eq. (38), obtained from Fig. 6, we see that the exponent α_{n_e} changes with density, being smaller at smaller density values.

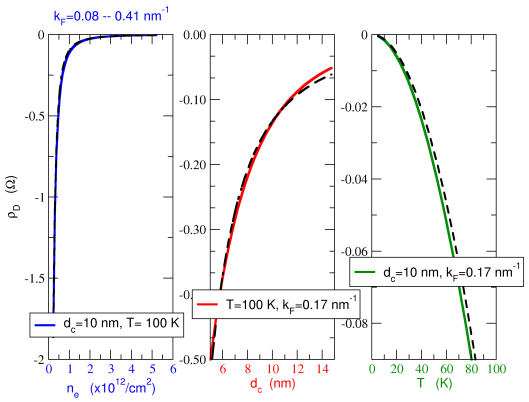

Fig. 6: Dependence of the drag resistivity as function of the electronic density, n_e, the interlayer distance, d_c, and the temperature, T. The used value of α is $\alpha = 0.21$

Acknowledgments. – We thank useful discussions with A. Geim and K. Novoselov. AHCN acknowledges DOE grant DE-FG02-08ER46512 and ONR grant MURI N00014-09-1-1063.

REFERENCES

[1] Rojo A. G., *J. Phys.: Condens. Matter* , **11** (1999) R31.

[2] Solomon P. M., Price P. J., Frank D. J. and La Tulipe D. C., *Phys. Rev. Lett.* , **63** (1989) 2508.
[3] Gramila T. J., Eisenstein J. P., MacDonald A. H., Pfeiffer L. N. and West K. W., *Phys. Rev. Lett.* , **66** (1991) 1216.
[4] Gramila T. J., Eisenstein J. P., MacDonald A. H., Pfeiffer L. N. and West K. W., *Physica B* , **197** (1994) 442.
[5] Novoselov K. S., Geim A. K., Morozov S. V., Jiang D., Zhang Y., Dubonos S. V., Grigorieva I. V. and Firsov A. A., *Science* , **306** (2004) 666.
[6] A. K. Geim, private communication.
[7] Kim S., Jo I., Nah J., Yao Z., Banerjee S. K. and Tutuc E., *Phys. Rev. B* , **83** (2011) 161401.
[8] Martin J., Akerman N., Ulbricht G., Lohmann T., Smet J. H., von Klitzing K. and Yacoby A., *Nature Phys.* , **4** (2008) 144.
[9] Zhang Y., Brar V. W., Girit C., Zettl A. and Crommie M. F., *Nature Phys.* , **5** (2009) 722.
[10] Tse W.-K., Hu B. Y.-K. and Das Sarma S., *Phys. Rev. B* , **76** (2007) 081401.
[11] Narozhny B. N., *Phys. Rev. B* , **76** (2007) 153409.
[12] Laikhtman B. and Solomon P. M., *Phys. Rev. B* , **41** (1990) 9921.
[13] Solomon P. M. and Laikhtman B., *Superlattices and Microstructures* , **10** (1991) 89.
[14] Jauho A.-P. and Smith H., *Phys. Rev. B* , **47** (1993) 4420.
[15] Flensberg K. and Hu B. Y.-K., *Phys. Rev. Lett.* , **73** (1994) 3572.
[16] Flensberg K. and Hu B. Y.-K., *Phys. Rev. B* , **52** (1995) 14796.
[17] Peres N. M. R., *Rev. Mod. Phys.* , **82** (2010) 2673.
[18] Abergel D. S. L., Apalkov V., Berashevich J., Ziegler K., Chakraborty T., *59*, **2010** (261)
[19] Dean C. R., Young A. F., Meric I., Lee C., Wang L., Sorgenfrei S., Watanabe K., Taniguchi T., Kim P., Shepard K. and Hone J., *Nature Nanotechnology* , **5** (2010) 722.
[20] Das Sarma S. and Hwang E. H., *Phys. Rev. B* , **83** (2011) 121405.
[21] Kim S., Nah J., Jo I., Shahrjerdi D., Colombo L., Yao Z., Tutuc E., and Banerjee S. K., *Appl. Phys. Lett.* , **94** (2009) 062107.
[22] Liao L., Bai J., Qu Y., chen Lin Y., Li Y., Huang Y. and Duan X., *PNAS* , **107** (2010) 6711.
[23] Reed J. P., Uchoa B., Il Joe1 Y., Gan Y., Casa D., Fradkin E. and Abbamonte P., *Science* , **320** (2010) 805.
[24] Ziman J. M., *Principles of the Theory of Solids* 2nd Edition (Cambridge University Press) 1979.
[25] Uchoa B. and Castro Neto A. H., *Phys. Rev. Lett.* , **98** (2007) 146801.
[26] Wunsch J. B., Stauber T., Sols F. and Guinea F., *New J. Phys.* , **8** (2006) 318.